ADVANCED MATERIALS INTERFACES

Supporting Information

for *Adv. Mater. Interfaces,* DOI: 10.1002/admi.202200430

Enabling Tunable Water-Responsive Surface Adaptation of PDMS via Metal–Ligand Coordinated Dynamic Networks

*Xinyue Zhang, Ralph Crisci, John A. Finlay, Hongyi Cai, Anthony S. Clare, Zhan Chen, and Meredith N. Silberstein**

Supporting Information

Enabling Tunable Water-Responsive Surface Adaptation of PDMS via Metal-ligand Coordinated Dynamic Networks

Xinyue Zhang,[a] Ralph Crisci,[b] John A. Finlay,[c] Hongyi Cai,[a] Anthony S. Clare,[c] Zhan Chen,[b] Meredith N. Silberstein[d*]

[a] Department of Materials Science and Engineering, Cornell University, Ithaca, New York 14853, United States

[b] Department of Chemistry, University of Michigan, Ann Arbor, Michigan 48109, United States

[c] School of Natural and Environmental Sciences, Newcastle University, Newcastle Upon Tyne, NE1 7RU, United Kingdom

[d] Sibley School of Mechanical and Aerospace Engineering, Cornell University, Ithaca, New York 14853, United States. Email: meredith.silberstein@cornell.edu

Table of Contents

S1. ^{1}H nuclear magnetic resonance (^{1}H NMR)

The structure of PI and DIP were characterized by ^{1}H NMR.

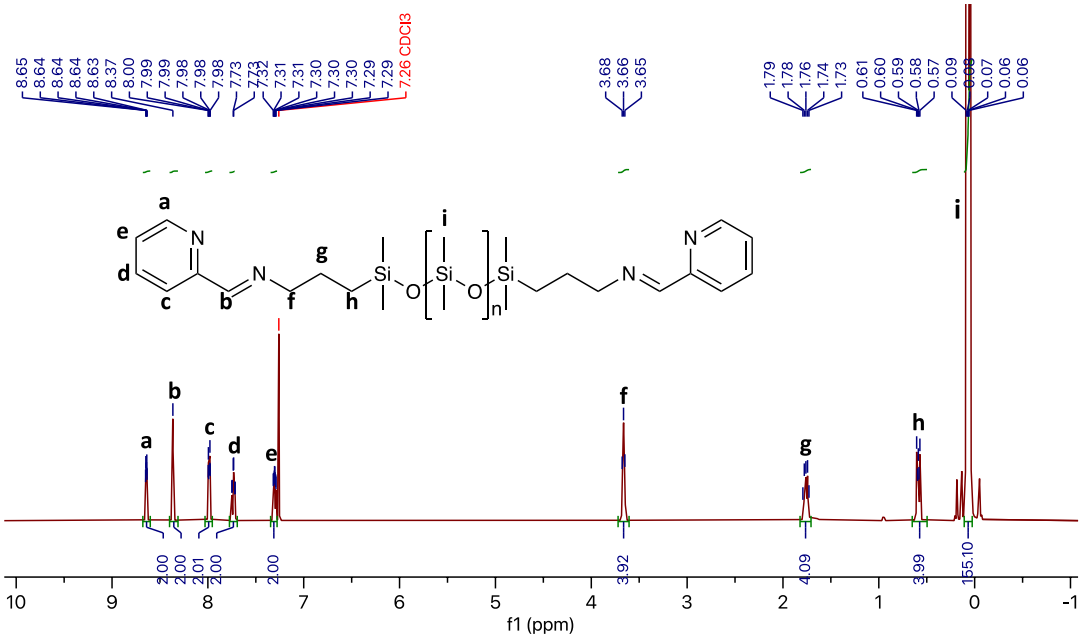

Figure S1 ^{1}H NMR spectrum of PI.

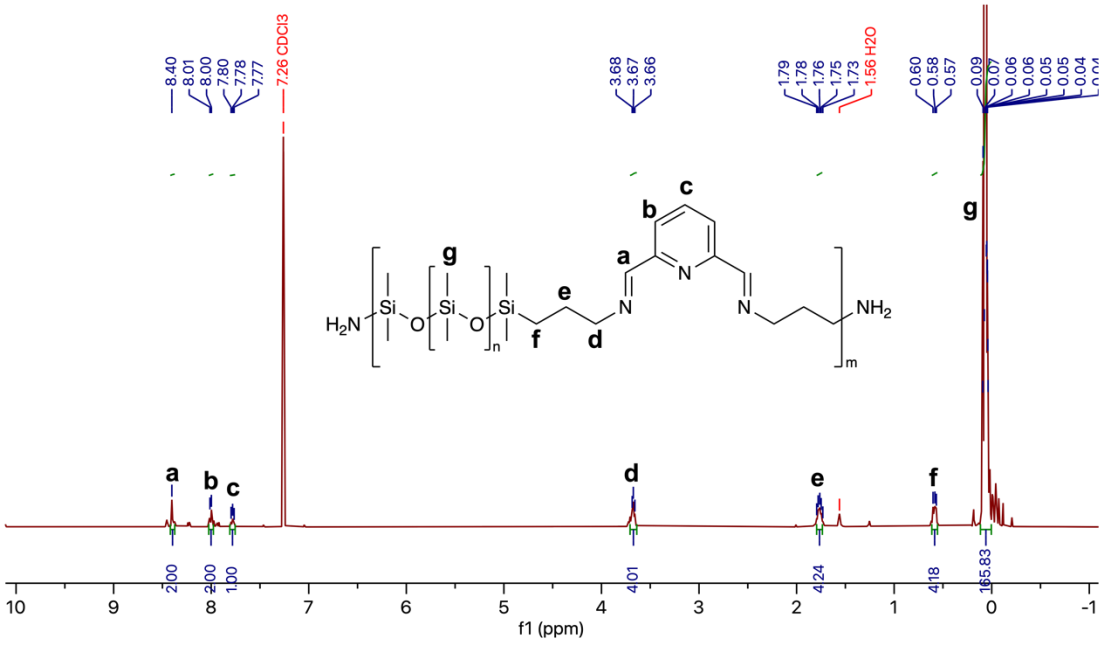

Figure S2 ^{1}H NMR spectrum of DIP.

S2. Gel permeation chromatography

The molecular weight and polydispersity of PI and DIP were measured by GPC. The number average molecular weight (M_n) of PI is ~2000 g/mol and polydispersity (*PDI*) is 1.3. The number average molecular weight (M_n) of DIP is ~9600 g/mol and polydispersity (*PDI*) is 1.6.

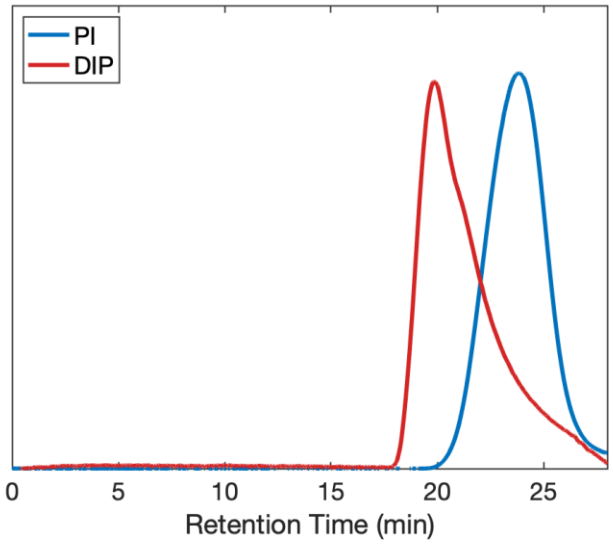

Figure S3. GPC spectra of PI and DIP.

S3. Mechanical and contact angle results for different network structures

Table S1. Young's moduli of PI-$Zn(BF_4)_2$ and DIP-$Zn(BF_4)_2$.

	PI-$Zn(BF_4)_2$	DIP-$Zn(BF_4)_2$
Young's modulus (MPa)	0.08 ± 0.01	13.88 ± 0.81

Table S2. Contact angle change over 20 mins for commercial PDMS, PI-$Zn(BF_4)_2$, and DIP-$Zn(BF_4)_2$.

	OOMOO® 30 PDMS (°)	PI-$Zn(BF_4)_2$ (°)	DIP-$Zn(BF_4)_2$ (°)
Start	104.9 ± 4.0	110.2 ± 4.0	110.7 ± 4.4
1 min	104.6 ± 2.7	108.6 ± 3.5	110.4 ± 4.5
2 min	103.8 ± 3.0	106.6 ± 3.9	110.0 ± 4.5
3 min	103.5 ± 2.9	103.8 ± 3.6	109.5 ± 4.4
4 min	103.2 ± 2.6	101.2 ± 2.8	109.0 ± 4.2
5 min	101.4 ± 2.6	98.6 ± 2.8	108.5 ± 4.0
10 min	100.0 ± 2.3	88.7 ± 3.5	106.2 ± 4.3
15 min	97.7 ± 2.9	81.0 ± 3.2	103.7 ± 4.5
20 min	94.9 ± 2.5	73.9 ± 3.8	100.9 ± 4.6

Table S3. Droplet volume change (% of the initial volume) in 20 mins for commercial PDMS, PI-$Zn(BF_4)_2$, and DIP-$Zn(BF_4)_2$.

	OOMOO® 30 PDMS	PI-$Zn(BF_4)_2$	DIP-$Zn(BF_4)_2$
Start	1.00 ± 0.00	1.00 ± 0.00	1.00 ± 0.00
1 min	1.00 ± 0.02	0.98 ± 0.01	0.99 ± 0.00
2 min	0.99 ± 0.02	0.97 ± 0.02	0.98 ± 0.00
3 min	0.97 ± 0.02	0.95 ± 0.02	0.96 ± 0.00
4 min	0.96 ± 0.02	0.93 ± 0.03	0.94 ± 0.01
5 min	0.95 ± 0.02	0.91 ± 0.02	0.93 ± 0.01
10 min	0.90 ± 0.04	0.83 ± 0.02	0.88 ± 0.00
15 min	0.84 ± 0.02	0.76 ± 0.03	0.82 ± 0.00
20 min	0.78 ± 0.01	0.69 ± 0.05	0.76 ± 0.00

S4. Study of environmental humidity effect

To create a humidity contrast in the ambient environment, we further equilibrated the PI-$Zn(BF_4)_2$ coated glass slides at a relative humidity of 85% using the saturated KCl/water solution, and measured the initial contact angle of water on the equilibrated surface (Table S4). The slightly decreased water contact angle indicates that the surface tends to be more hydrophilic in the environment with higher relative humidity.

Table S4. Initial contact angle of PI-$Zn(BF_4)_2$ at different relative humidity (RH).

	RH~40%, lab environment	RH~85%, equilibrated by KCl solution
Initial contact angle (°)	110.2 ± 4.0	106.1 ± 2.5

S5. Study of triggering surface adaptation by other liquids

To verify the idea that the surface adaptation could be triggered by other polar liquids besides water, we performed contact angle measurements using ethylene glycol. As seen from the contact angle evolution, ethylene glycol triggers a similar hydrophilic evolution on the PI-$Zn(BF_4)_2$ surface as water does (Figure S4). Moreover, ethylene glycol has a high boiling point (197 ℃), and therefore evaporates much slower than water in the ambient environment, so the volume of the ethylene glycol droplets does not change in the 20 min (Figure S5). The expansion of the contact area of ethylene glycol further confirms the increase of hydrophilicity on the PI-$Zn(BF_4)_2$ surface.

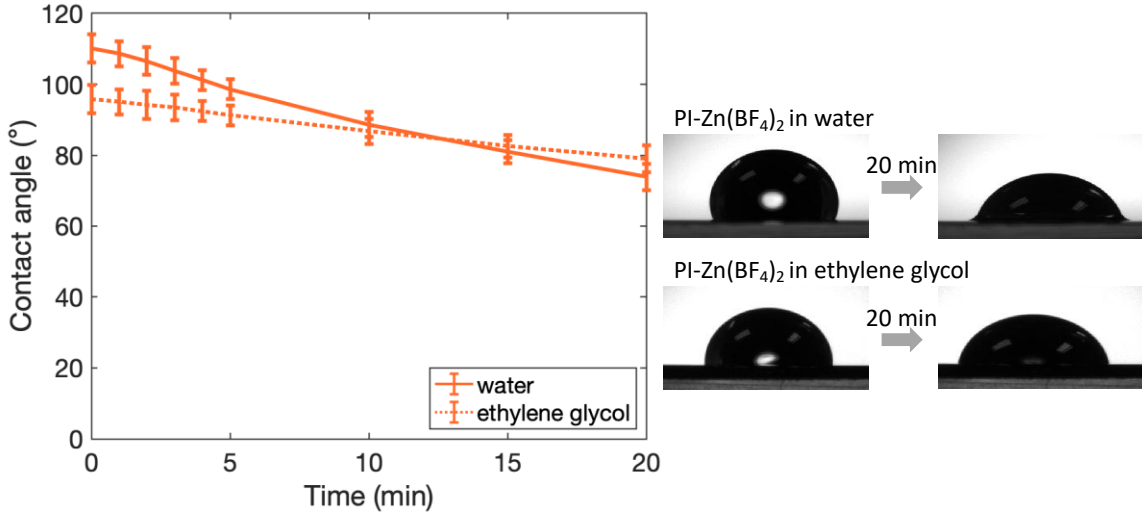

Figure S4. Change of the water contact angle on the PI-$Zn(BF_4)_2$ surface using water and ethylene glycol and photos of the interface upon droplet application and after 20 min. Each data point plotted is the mean value measured from three different spots, and bars show the standard deviation.

Table S5. Contact angle change over 20 mins for PI-$Zn(BF_4)_2$ using ethylene glycol.

	PI-$Zn(BF_4)_2$ with ethylene glycol (°)
Start	95.9 ± 1.5
1 *min*	95.1 ± 1.4
2 *min*	94.2 ± 1.2
3 *min*	93.4 ± 0.8
4 *min*	92.4 ± 0.8
5 *min*	91.3 ± 0.6
10 *min*	86.7 ± 0.2
15 *min*	82.6 ± 0.5
20 *min*	79.0 ± 0.7

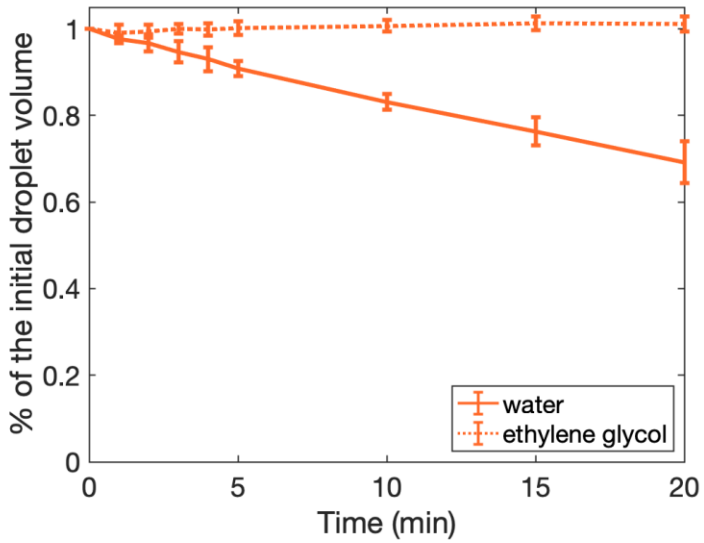

Figure S5. Change of the droplet volume on PI-Zn$(BF_4)_2$. Each data point plotted is the mean value measured from three different spots, and bars show the standard deviation.

Table S6. Droplet volume change (% of the initial volume) in 20 mins for ethylene glycol on the PI-Zn$(BF_4)_2$ surface.

	PI-Zn$(BF_4)_2$ with ethylene glycol (°)
Start	1.00 ± 0.00
1 min	0.99 ± 0.02
2 min	0.99 ± 0.02
3 min	1.00 ± 0.01
4 min	1.00 ± 0.01
5 min	1.00 ± 0.02
10 min	1.00 ± 0.01
15 min	1.01 ± 0.02
20 min	1.01 ± 0.02

A clear contrast could be seen when applying a non-polar liquid. We performed contact angle measurements using silicone oil. The droplets spread out on all the PDMS surfaces fast and form an almost perfect wetting due to the similar surface tension between the silicone oil and the PDMS. A typical picture is shown below.

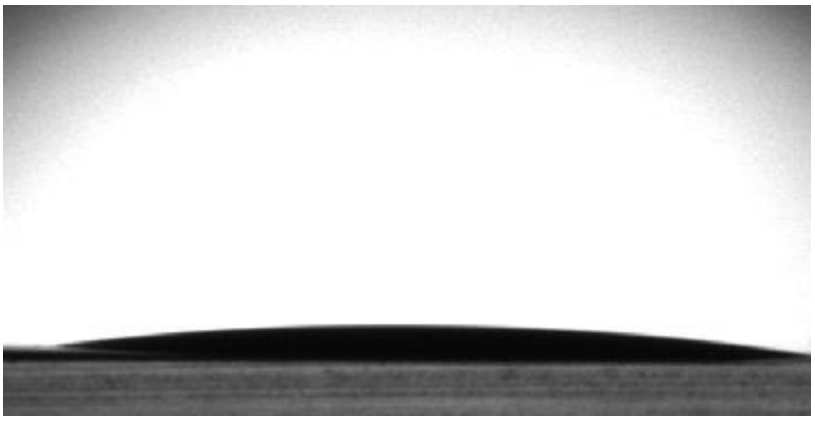

Figure S6. A photo of the interface after applying a silicone oil droplet on PI-$Zn(BF_4)_2$.

S6. Reversibility of the surface adaptation

To verify that the hydrophilic-adapted metal-coordinated PI surface would restore its hydrophobicity in air, we immersed a newly made PI-$Zn(BF_4)_2$ coated glass in water for 2 hr to develop a hydrophilic surface, and then took it out and dried the glass slide under vacuum to completely remove water. The wet-dry procedure was repeated 3 time. We measured the surface contact angle at multiple spots in each step and compared the results.

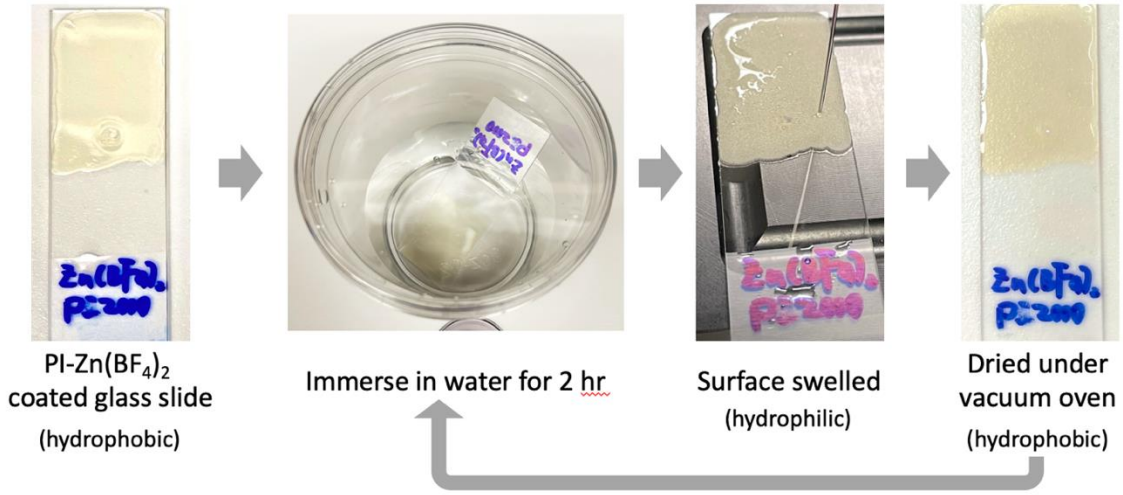

Figure S7. Experimental procedures of testing the surface reversibility.

Table S7. Contact angle result during each wet-dry cycle.

Wet-dry procedure	Contact angle (°)	
	On the dried surface	On the swelled surface*
Newly made sample	107.44 ± 1.80	65.80 ± 11.32
2nd cycle	108.87 ± 1.58	68.83 ± 17.29
3rd cycle	107.89 ± 1.05	67.91 ± 16.38

*Note: a large contact angle heterogeneity is observed on the swelled surface due to both the uneven surface topology and some water residue on discrete areas.

S7. SFG Study on different network structures

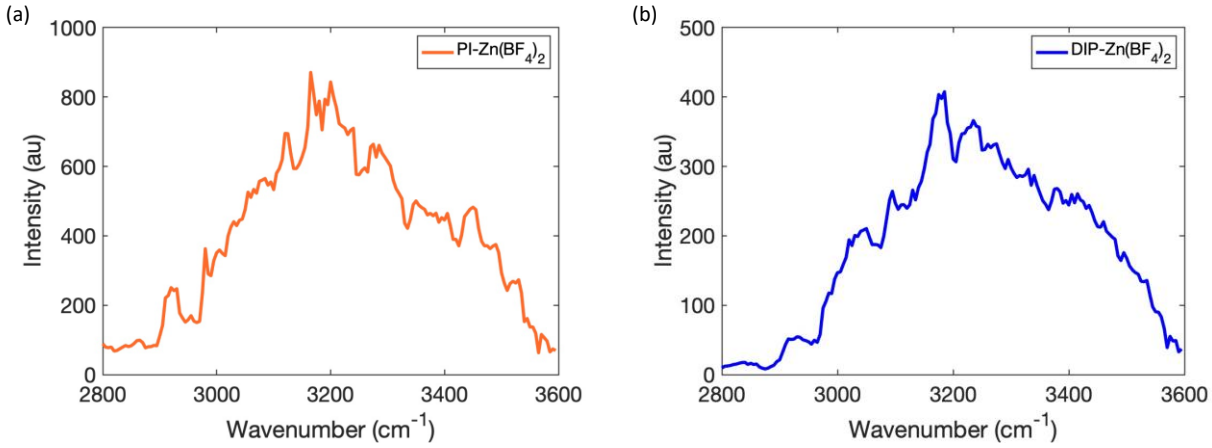

Figure S8. SFG spectra in water: (a) PI-$Zn(BF_4)_2$, (b) DIP-$Zn(BF_4)_2$.

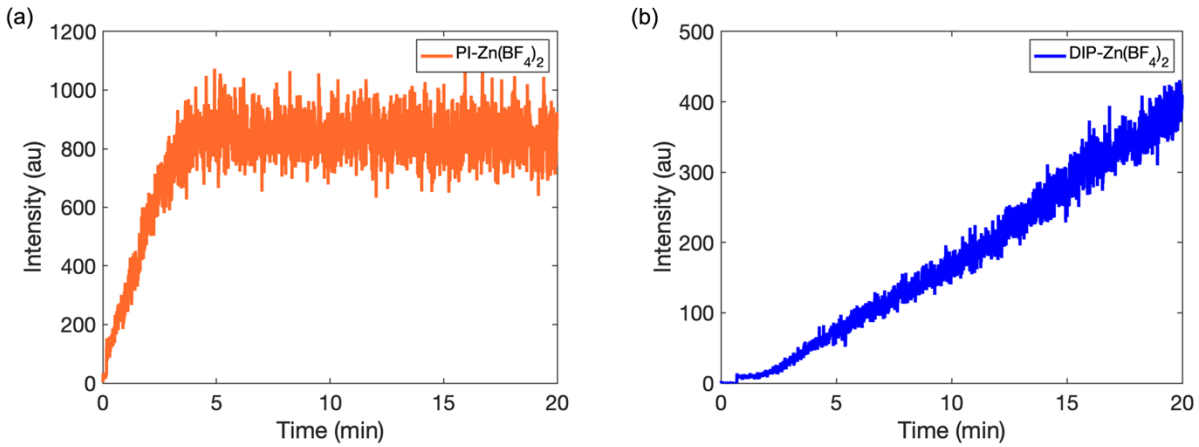

Figure S9. Time-dependent SFG signal in water: (a) PI-$Zn(BF_4)_2$, (b) DIP-$Zn(BF_4)_2$. Please note that these spectra and time-dependent signals are replots of those shown in Figure 2f and 2g in the main text with different y-axis scales. In the main text, the y-axis has the same scale to facilitate the comparison of SFG signal intensities. Here different y-axis scales are used for different plots to better observe the SFG spectral features and time-dependent signal changes.

S8. Study of different counter anions

The FTIR spectra were normalized by the absorption peak of Si-CH_3 bending at 1260 cm^{-1}. For all three Zn(II)-coordinated PI, the C=N stretching peaks at 1650 cm^{-1} decrease and new peaks arise at ~1590 cm^{-1}, due to the shift of absorption band resulted from bond order decreasing.

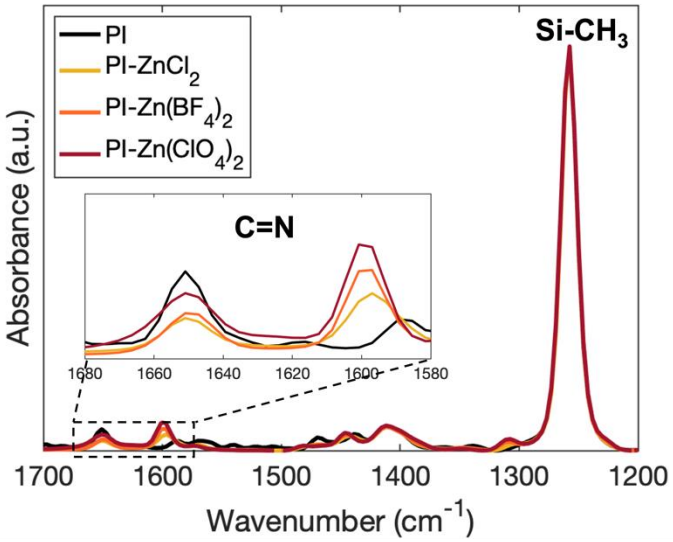

Figure S10. FTIR of the Zn(II)-coordinated PI.

Table S8. Young's moduli of PI-$Zn(ClO_4)_2$.

	PI-$Zn(ClO_4)_2$
Young's modulus (MPa)	1.36 ± 0.01

Table S9. Characteristic relaxation time of the material/coordination lifetime of Zn(II)-PI under different counter anions determined from rheology.

	PI-$ZnCl_2$	PI-$Zn(BF_4)_2$	PI-$Zn(ClO_4)_2$
Characteristic relaxation time/ coordination lifetime (s)	0.03 ± 0.01	0.24 ± 0.06	6.31 ± 0.00

Table S10. Contact angle change over 20 mins for PI-$ZnCl_2$ and PI-$Zn(ClO_4)_2$.

	PI-$ZnCl_2$	PI-$Zn(ClO_4)_2$
Start	120.7 ± 0.4	103.9 ± 2.2
1 min	57.1 ± 2.5	103.5 ± 2.2
2 min	48.0 ± 1.4	103.3 ± 2.1
3 min	43.8 ± 2.2	103.0 ± 2.3
4 min	40.9 ± 2.0	102.7 ± 2.4
5 min	39.0 ± 2.4	102.3 ± 2.7
10 min	33.7 ± 1.9	99.1 ± 2.4
15 min	30.2 ± 1.8	94.6 ± 2.1
20 min	27.5 ± 1.9	91.1 ± 1.9

Table S11. Droplet volume change (% of the initial volume) over 20 mins for PI-$ZnCl_2$ and PI-$Zn(ClO_4)_2$.

	PI-$ZnCl_2$	PI-$Zn(ClO_4)_2$
Start	1.00 ± 0.00	1.00 ± 0.00
1 min	0.96 ± 0.01	0.99 ± 0.00
2 min	0.93 ± 0.00	0.97 ± 0.00
3 min	0.91 ± 0.01	0.96 ± 0.01
4 min	0.89 ± 0.00	0.95 ± 0.01
5 min	0.86 ± 0.01	0.93 ± 0.01
10 min	0.77 ± 0.00	0.86 ± 0.01
15 min	0.72 ± 0.01	0.78 ± 0.02
20 min	0.65 ± 0.00	0.72 ± 0.01

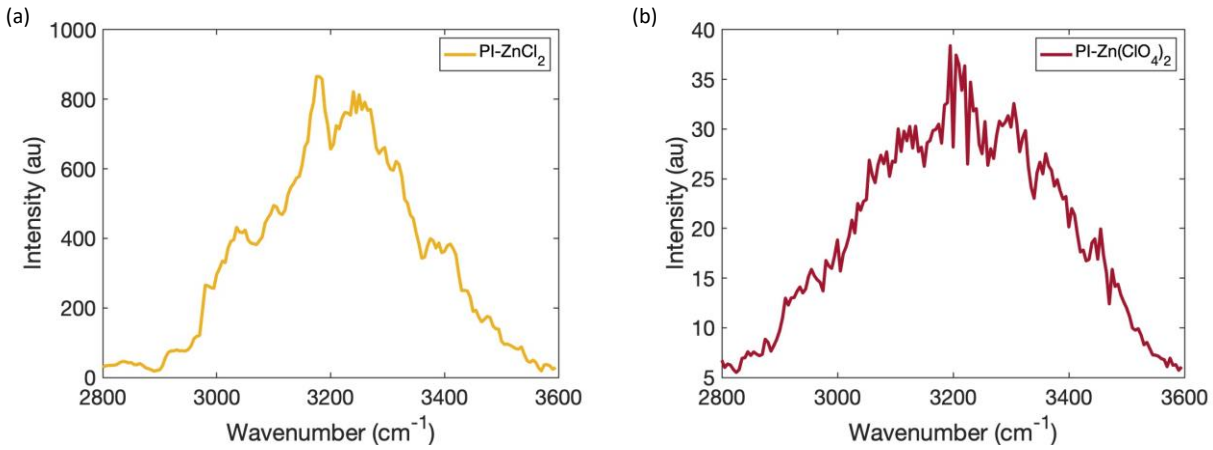

Figure S11. SFG spectra in water: (a) PI-$ZnCl_2$, (b) PI-$Zn(ClO_4)_2$.

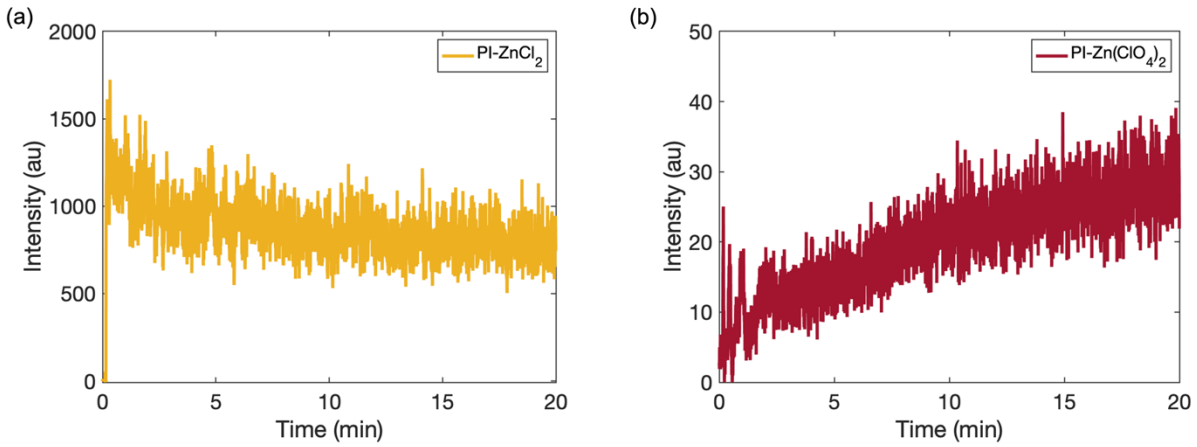

Figure S12. Time-dependent SFG signal in water: (a) PI-$ZnCl_2$, (b) PI-$Zn(ClO_4)_2$. Please note that these spectra and time-dependent signals are replots of those of PI-$ZnCl_2$ and PI-$Zn(ClO_4)_2$ shown in Figure 3f and 3g in the main text with different y-axis scales. In the main text, the y-axis has the same scale to facilitate the comparison of SFG signal intensities. Here different y-axis scales are used for different plots to better observe the SFG spectral features and time-dependent signal changes.

S9. Study of different metal cations with octahedral coordination

The FTIR spectra were normalized by the absorption peak of Si-CH_3 bending at 1260 cm^{-1}. For all three metal-coordinated PI, the C=N stretching peaks at 1650 cm^{-1} decrease and new peaks arise at ~1610 cm^{-1} for the Fe(II) coordinated PI and at ~1600 cm^{-1} for the Fe(II) coordinated PI, due to the shift of absorption band resulted from bond order decreasing.

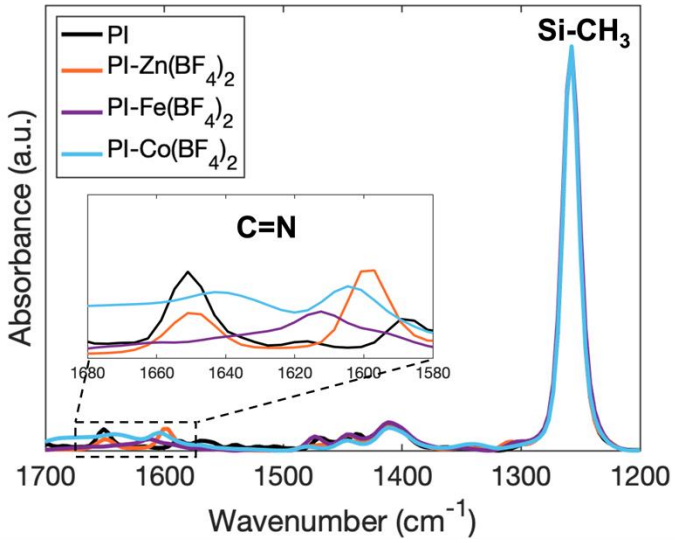

Figure S13. FTIR of the PI coordinated by different metal cations.

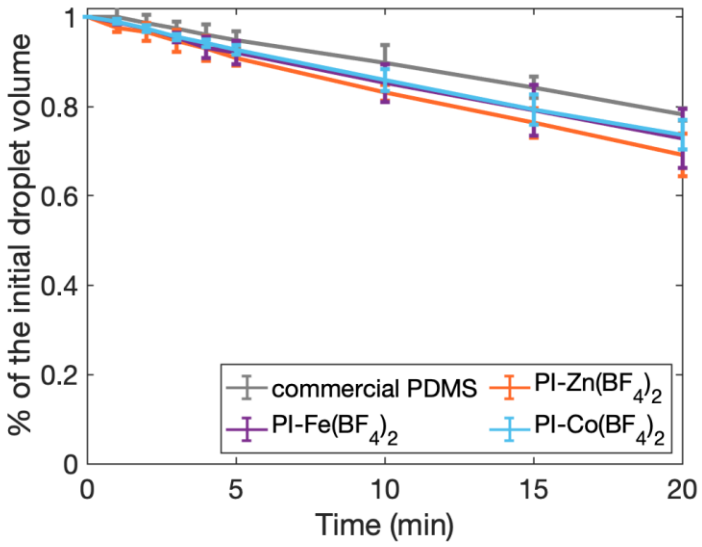

Figure S14. Change of water droplet volume. Each data point plotted is the mean value measured from three different spots, and bars show the standard deviation.

Table S12. Young's moduli of PI-$Fe(BF_4)_2$ and PI-$Co(BF_4)_2$.

	PI-$Fe(BF_4)_2$	PI-$Co(BF_4)_2$
Young's modulus (MPa)	0.29 ± 0.04	3.32 ± 0.32

Table S13. Contact angle change over 20 mins for PI-$Fe(BF_4)_2$ and PI-$Co(BF_4)_2$.

	PI-$Fe(BF_4)_2$ (°)	PI-$Co(BF_4)_2$ (°)
Start	107.8 ± 1.4	105.9 ± 1.9
1 min	106.7 ± 1.0	105.7 ± 1.9
2 min	105.4 ± 1.2	105.3 ± 1.8
3 min	103.6 ± 1.1	104.9 ± 2.0
4 min	102.1 ± 1.5	104.4 ± 2.2
5 min	101.0 ± 1.6	104.0 ± 2.2
10 min	93.8 ± 3.0	101.2 ± 2.7
15 min	87.9 ± 4.0	97.8 ± 3.5
20 min	81.5 ± 4.5	95.4 ± 2.8

Table S14. Droplet volume changing (% of the initial volume) over 20 mins for PI-$Fe(BF_4)_2$ and PI-$Co(BF_4)_2$.

	PI-$Fe(BF_4)_2$	PI-$Co(BF_4)_2$
Start	1.00 ± 0.00	1.00 ± 0.00
1 min	0.99 ± 0.00	0.99 ± 0.00
2 min	0.97 ± 0.01	0.97 ± 0.01
3 min	0.95 ± 0.01	0.96 ± 0.01
4 min	0.93 ± 0.02	0.94 ± 0.01
5 min	0.92 ± 0.03	0.93 ± 0.01
10 min	0.85 ± 0.04	0.86 ± 0.02
15 min	0.79 ± 0.06	0.79 ± 0.03
20 min	0.73 ± 0.07	0.74 ± 0.03

SFG was also used to study the effects of metal ions on the surface behavior of PDMS materials. SFG spectra are collected from PI-Co$(BF_4)_2$ in air, in water, and time-dependent signal change in water (Figure S11, Figure S12 and Figure S13). For comparison, the SFG spectra and time-dependent signals from PI-Zn$(BF_4)_2$ are also shown in these figures. The SFG spectrum collected from PI-Co$(BF_4)_2$ in air does not show any C-H stretching signals, showing disordered CH groups on the surface in air. This is very different from that collected from PI-Zn$(BF_4)_2$ and other two PI-Zn(II) surfaces in air. As discussed in the manuscript, PI-Co$(BF_4)_2$ has the strongest coordination strength and the least dynamic PDMS network among the PI system coordinated with BF_4^- anions, leading to a more rigid bulk as well as surface structure. Therefore, even though air is hydrophobic, the hydrophobic CH groups are not able to segregate to the surface to dominate the surface with order on the PI-Co$(BF_4)_2$ surface. The more hydrophobic PI-Co$(BF_4)_2$ surface in water can also be seen from the much weaker SFG water signal collected from the PI-Co$(BF_4)_2$/water interface compared to that collected from the PI-Zn$(BF_4)_2$/water interface. This can also explain the very different water contact angles measured on the PI-Co$(BF_4)_2$ and PI-Zn$(BF_4)_2$ surfaces. Furthermore, the PI-Co$(BF_4)_2$ time-dependent surface structural change in water is less dramatic than PI-Zn$(BF_4)_2$, evidenced by the SFG signal intensities observed as a function of time from the PI-Co$(BF_4)_2$/water interface is weaker than that from the PI-Zn$(BF_4)_2$/water interface.

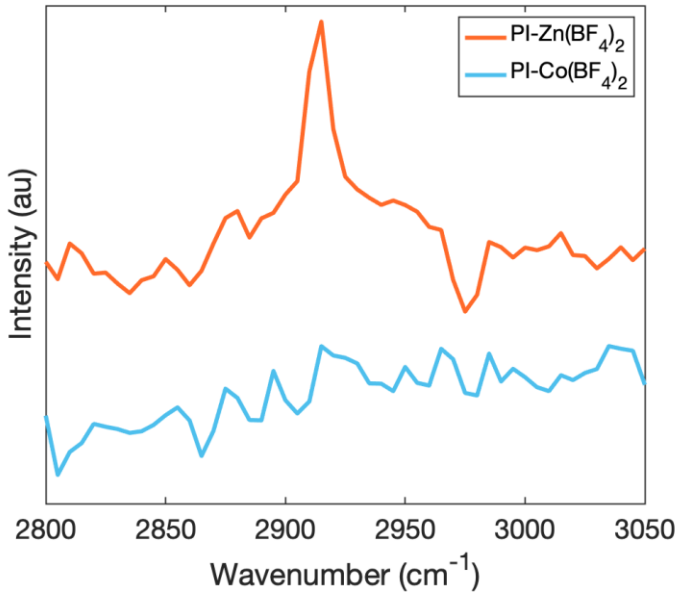

Figure S15. SFG spectra in air.

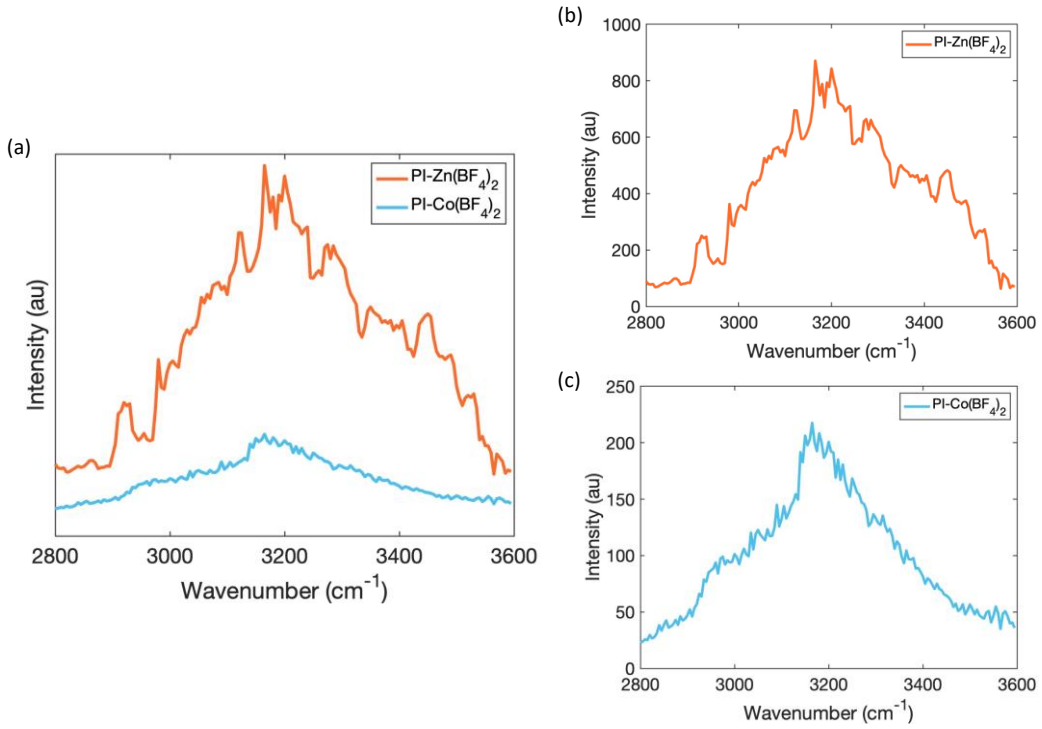

Figure S16. SFG spectra in water: (a) plotted on the same graph with offset; (b) and (c) plotted individually.

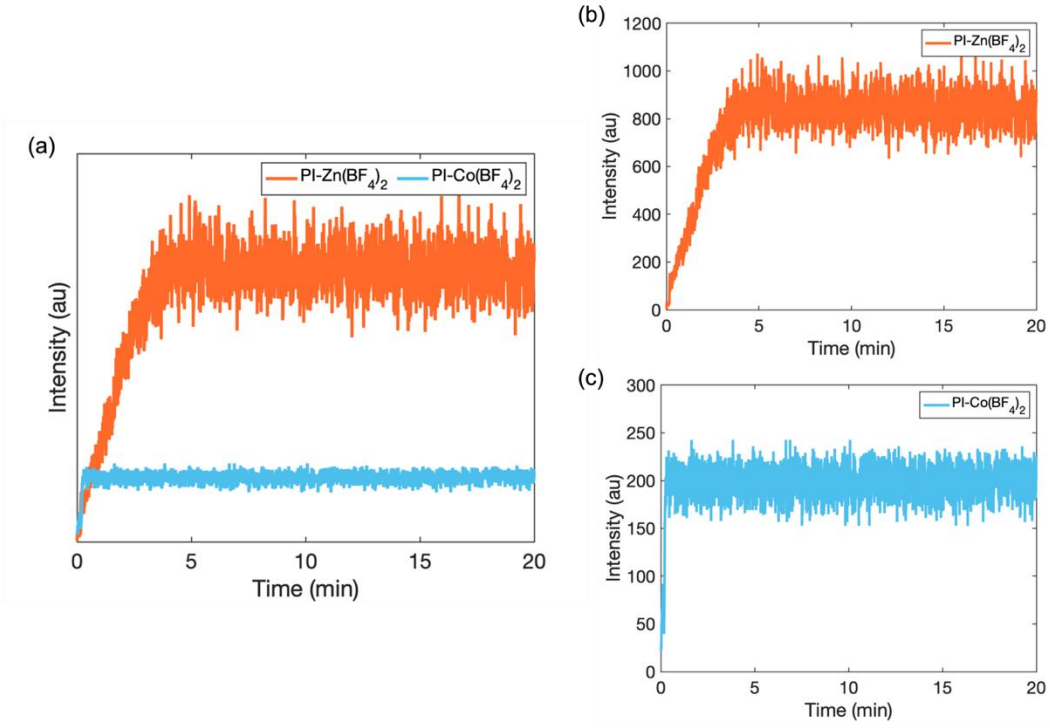

Figure S17. Time-dependent SFG signal in water: (a) plotted on the same graph with offset; (b) and (c) plotted individually.

S10. Long time wetting

To evaluate the contact angle change of water droplets in longer time, we made a chamber to maintain the humidity equilibrium. As show in Figure S8, a PDMS coated glass slide is floating on small amount of water in a petri dish. Several water droplets were placed on the coating surface. The petri dish was capped, with a Pyrex® circular glass dish covering outside.

The contact angle of the droplets was measured after 24 hr.

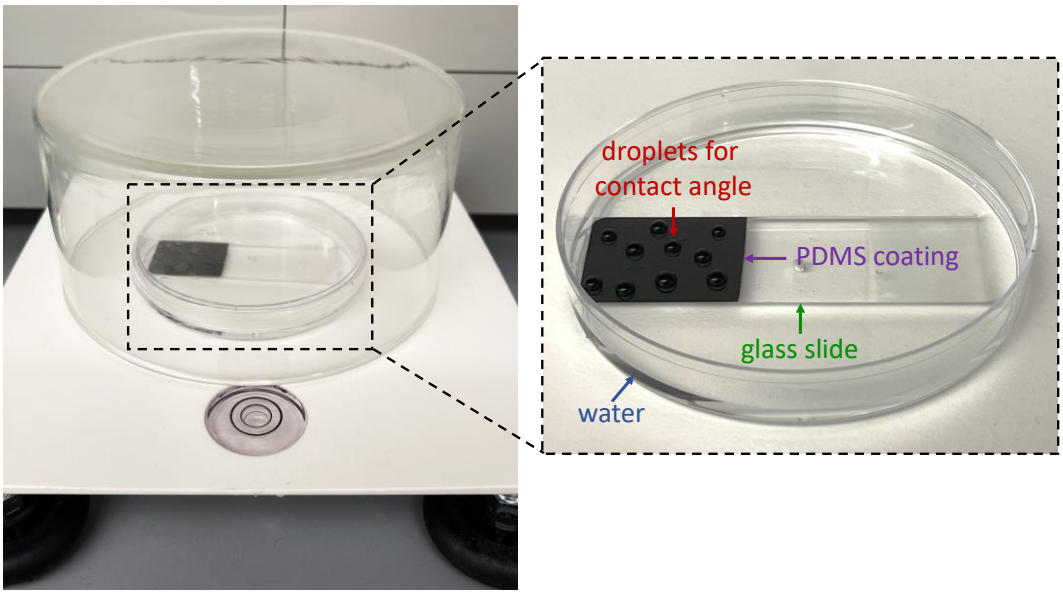

Figure S18. Humidity chamber setup.

Table S15. Contact angle change in 24 hr for PI-Fe$(BF_4)_2$ and PI-Co$(BF_4)_2$.

	PI-Fe$(BF_4)_2$ (°)	PI-Co$(BF_4)_2$ (°)
Start	107.8 ± 1.4	105.9 ± 1.9
24 *hr* (in the chamber)	34.4 ± 4.3	61.6 ± 7.7

S11. Study of Cu(II) cation with tetrahedral coordination

To verify that Cu(II) cations generate tetrahedral coordination geometry with pyridyl imine ligands, we synthesized the model ligand N-propyl(2-pyridyl)methanimine and characterized its structure by ^{1}H-NMR.

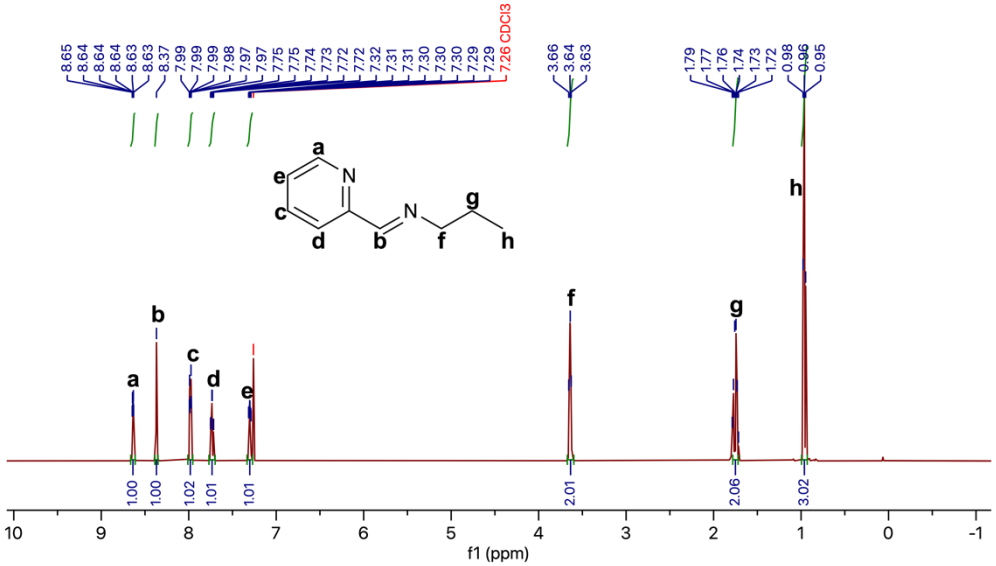

Figure S19. ^{1}H NMR spectrum of N-propyl(2-pyridyl)methanimine.

We next synthesized the $Cu(BF_4)_2$ coordinated N-propyl(2-pyridyl)methanimine salt and characterized the coordination stoichiometry by EIS-MS. The sample was diluted 1:10 times with 50% methanol and then using tee-in direct injection into the mass spectrometer with a flow rate of 200 μl/min. The flow rate of the sample through the syringe pump is 9 μl/min. In the MS analysis for identification, Sciex X500B was operated in ESI positive ion FT mode, and the calibration was done with positive calibrant using CDS system.

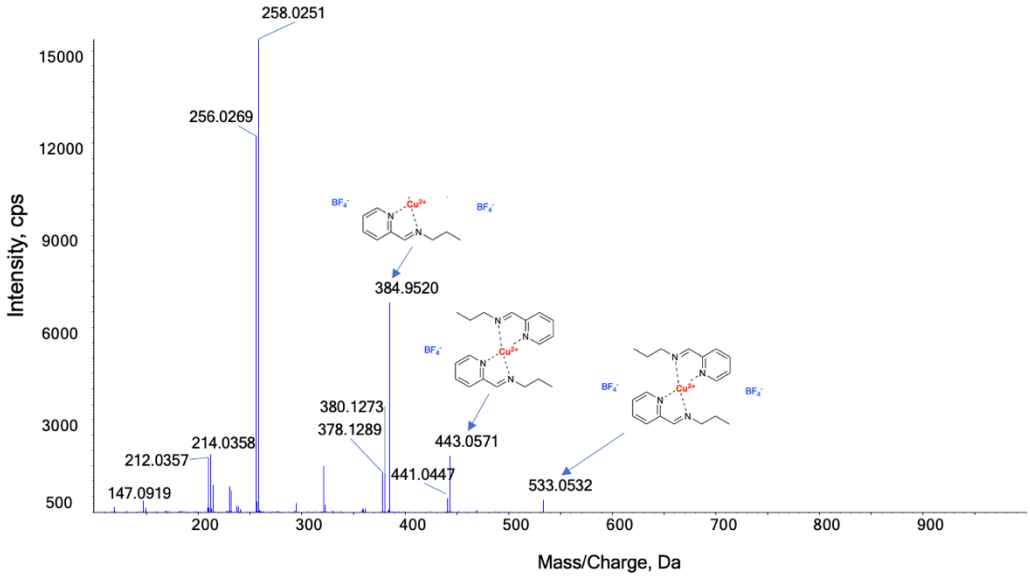

Figure S20. EIS-MS spectrum of N-propyl(2-pyridyl)methanimine.

The salt has the mass of 533.06, corresponding to the coordination ratio of $Cu(BF_4)_2$: N-propyl(2-pyridyl)methanimine = 1:2. Extra peaks are coming from solvent or from in source fragmentation.

The water contact angle measurements have been performed on the PI-$Cu(BF_4)_2$ surface.

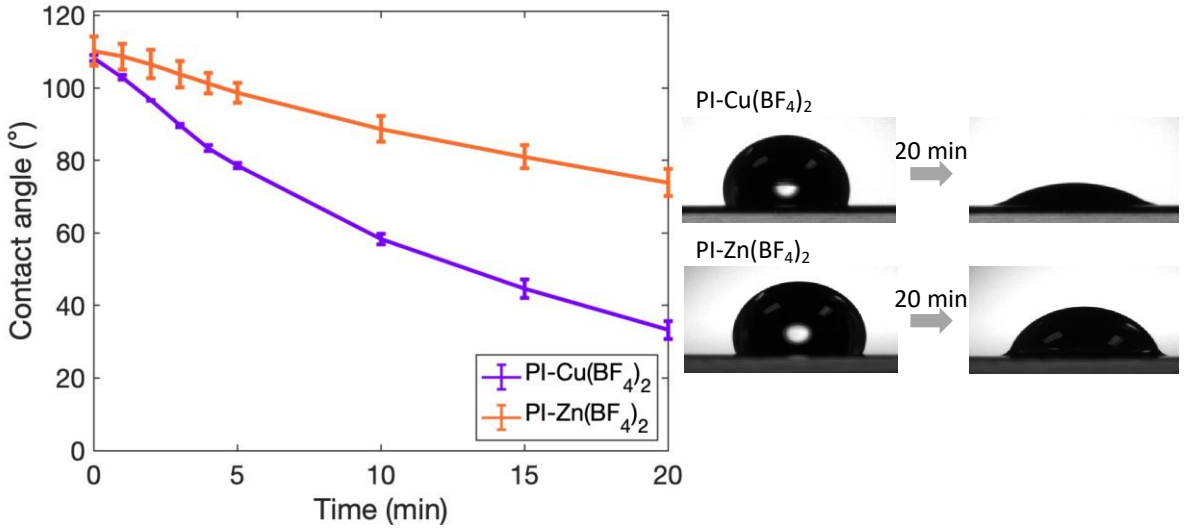

Figure S21. Change of the water contact angle on different PDMS surfaces and photos of the interface upon droplet attachment and after 20 min. Each data point plotted is the mean value measured from three different spots, and bars show the standard deviation.

Table S16. Contact angle change over 20 mins for PI-$Cu(BF_4)_2$.

	PI-$Cu(BF_4)_2$ (°)
Start	107.8 ± 1.4
1 *min*	106.7 ± 1.0
2 *min*	105.4 ± 1.2
3 *min*	103.6 ± 1.1
4 *min*	102.1 ± 1.5
5 *min*	101.0 ± 1.6
10 *min*	93.8 ± 3.0
15 *min*	87.9 ± 4.0
20 *min*	81.5 ± 4.5

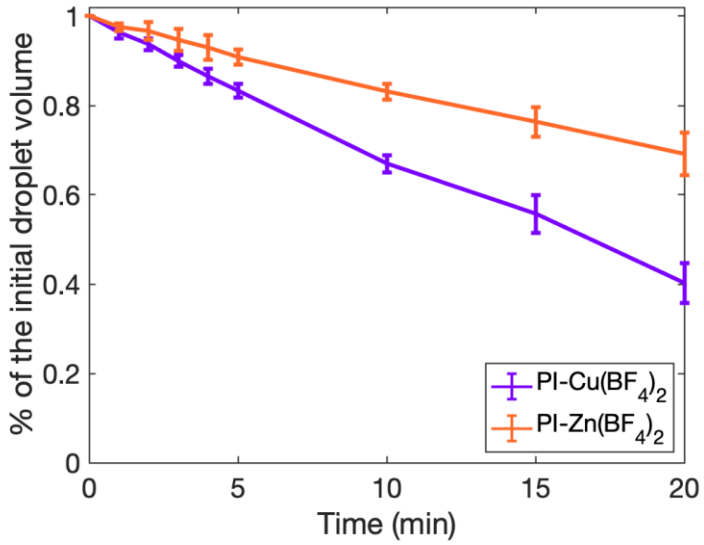

Figure S22. Change of the droplet volume on PI-Zn$(BF_4)_2$. Each data point plotted is the mean value measured from three different spots, and bars show the standard deviation.

Table S17. Droplet volume change (% of the initial volume) over 20 mins for PI-Cu$(BF_4)_2$.

	PI-Cu$(BF_4)_2$
Start	1.00 ± 0.00
$1\ min$	0.96 ± 0.01
$2\ min$	0.94 ± 0.01
$3\ min$	0.90 ± 0.01
$4\ min$	0.87 ± 0.02
$5\ min$	0.83 ± 0.02
$10\ min$	0.67 ± 0.02
$15\ min$	0.56 ± 0.04
$20\ min$	0.40 ± 0.04

S12. SFG study on antifouling coatings

To understand the different fouling release performance of DIP-$Co(BF_4)_2$, its interfacial molecular behavior was investigated using SFG. The SFG spectrum collected from the DIP-$Co(BF_4)_2$ surface in air (Figure S15) is similar to that collected from the DIP-$Zn(BF_4)_2$. Interestingly, the SFG spectrum collected in water (Figure S16) has a much weaker intensity compared to that collected from PI-$Co(BF_4)_2$ in water; also the SFG time-dependent signal does not have substantial change in water (Figure S17). This shows that DIP-$Co(BF_4)_2$ surface is even more hydrophobic in water, due to a less flexible surface caused by a stronger polymer network.

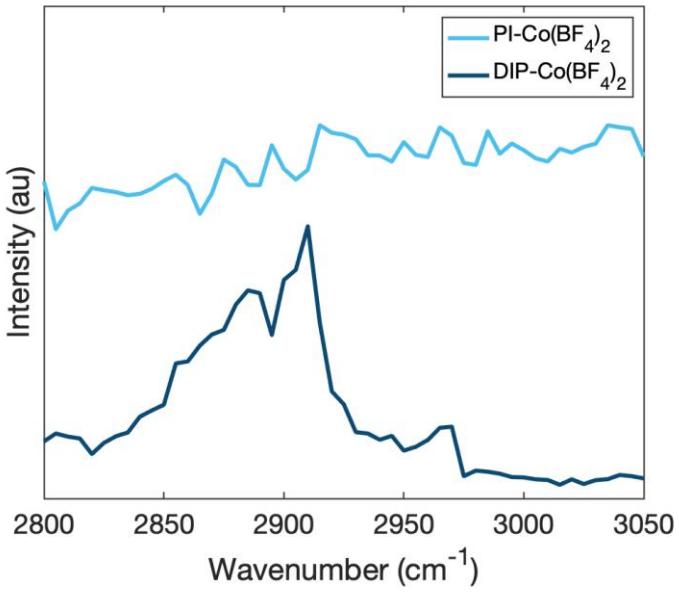

Figure S23. SFG spectra in air.

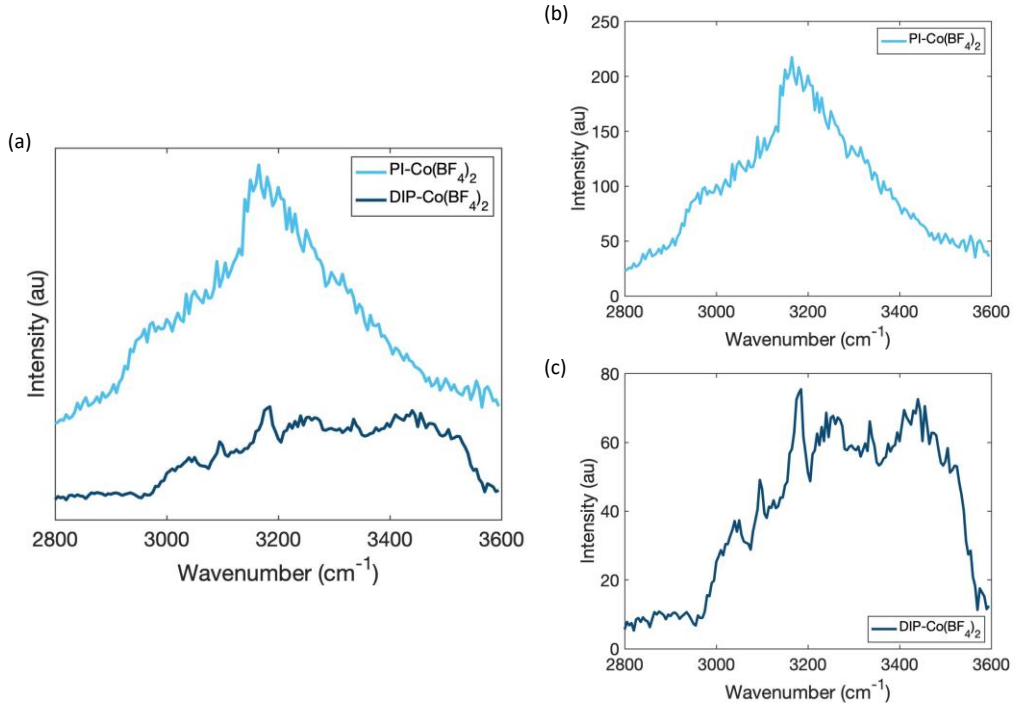

Figure S24. SFG spectra in water: (a) plotted on the same graph with offset; (b) and (c) plotted individually.

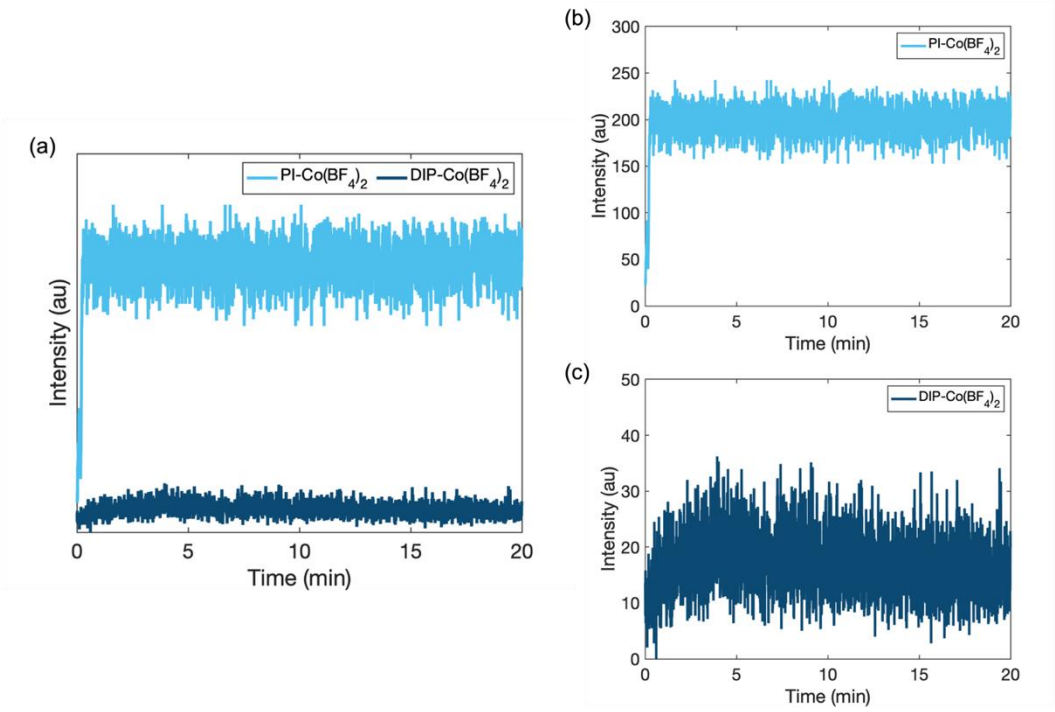

Figure S25. Time-dependent SFG signal in water: (a) plotted on the same graph with offset; (b) and (c) plotted individually.

S13. SI References

1. J. Pignanelli, B. Billet, M. Straeten, M. Prado, K. Schlingman, M. J. Ahamed and S. Rondeau-Gagné, *Soft Matter*, 2019, **15**, 7654–7662.

2. D.-P. Wang, J.-C. Lai, H.-Y. Lai, S.-R. Mo, K.-Y. Zeng, C.-H. Liand J.-L. Zuo, *Inorganic Chemistry*, 2018, **57**, 3232–3242.